

## Integrated device for combined optical neuromodulation and electrical recording for chronic *in vivo* applications

This article has been downloaded from IOPscience. Please scroll down to see the full text article.

2012 J. Neural Eng. 9 016001

(<http://iopscience.iop.org/1741-2552/9/1/016001>)

View [the table of contents for this issue](#), or go to the [journal homepage](#) for more

Download details:

IP Address: 171.65.95.177

The article was downloaded on 24/01/2012 at 02:36

Please note that [terms and conditions apply](#).

# Integrated device for combined optical neuromodulation and electrical recording for chronic *in vivo* applications

Jing Wang<sup>1</sup>, Fabien Wagner<sup>2</sup>, David A Borton<sup>3</sup>, Jiayi Zhang<sup>4</sup>,  
Ilker Ozden<sup>3</sup>, Rebecca D Burwell<sup>2,5</sup>, Arto V Nurmikko<sup>1,3</sup>,  
Rick van Wagenen<sup>6</sup>, Ilka Diester<sup>7</sup> and Karl Deisseroth<sup>7</sup>

<sup>1</sup> Department of Physics, Brown University, Providence, RI, USA

<sup>2</sup> Department of Neuroscience, Brown University, Providence, RI, USA

<sup>3</sup> School of Engineering, Brown University, Providence, RI, USA

<sup>4</sup> Department of Neurobiology, School of Medicine, Yale University, New Haven, CT, USA

<sup>5</sup> Department of Cognitive, Linguistic and Psychological Sciences, Brown University, Providence, RI, USA

<sup>6</sup> Blackrock Microsystems, Salt Lake City, UT, USA

<sup>7</sup> Department of Bioengineering, Stanford University, Stanford, CA, USA

E-mail: [Arto\\_Nurmikko@brown.edu](mailto:Arto_Nurmikko@brown.edu)

Received 9 May 2011

Accepted for publication 28 September 2011

Published 7 December 2011

Online at [stacks.iop.org/JNE/9/016001](http://stacks.iop.org/JNE/9/016001)

## Abstract

Studying brain function and its local circuit dynamics requires neural interfaces that can record and stimulate the brain with high spatiotemporal resolution. Optogenetics, a technique that genetically targets specific neurons to express light-sensitive channel proteins, provides the capability to control central nervous system neuronal activity in mammals with millisecond time precision. This technique enables precise optical stimulation of neurons and simultaneous monitoring of neural response by electrophysiological means, both in the vicinity of and distant to the stimulation site. We previously demonstrated, *in vitro*, the dual capability (optical delivery and electrical recording) while testing a novel hybrid device (optrode-MEA), which incorporates a tapered coaxial optical electrode (optrode) and a 100 element microelectrode array (MEA). Here we report a fully chronic implant of a new version of this device in ChR2-expressing rats, and demonstrate its use in freely moving animals over periods up to 8 months. In its present configuration, we show the device delivering optical excitation to a single cortical site while mapping the neural response from the surrounding 30 channels of the  $6 \times 6$  element MEA, thereby enabling recording of optically modulated single-unit and local field potential activity across several millimeters of the neocortical landscape.

 Online supplementary data available from [stacks.iop.org/JNE/9/016001/mmedia](http://stacks.iop.org/JNE/9/016001/mmedia)

(Some figures in this article are in colour only in the electronic version)

## 1. Introduction

Targeted spatiotemporal access to neural populations at single neuron resolution is important to the study of neural circuits and cellular conditions, both for basic understanding of their functions as well as developing approaches to many

classes of neuronal disorders. Modulating neural circuits by intracortical electrical stimulation is a well-established tool in electrophysiology and clinical neurosurgery, even if uncertainties are inherently present, given such non-selective activation of cells by the complex patterns of current flow [1]. In a broader context of the utility of

external neuromodulation methods, systematic models of how activity in neural circuits occurs, whether normal or aberrant, are made complicated by the nonspecific nature associated with electrical, magnetic and pharmacological targeting. A new approach to neural modulation occurred with the discovery of a light-sensitive ion channel, Channelrhodopsin-2 (ChR2) [2], followed by the discovery of an optically activated chloride pump, Halorhodopsin (NpHR) [3], and a proton pump, Archaeorhodopsin (Arch) [4]. Through the combination of genetic and optical methods these discoveries were rapidly advanced in mammalian animal models as fundamentally new methods for targeting neurons, now termed 'optogenetics' [5–8].

Light-induced modulation enables both neuronal excitation and inhibition, each for inducing well-defined neuronal events with millisecond time resolution [7]. Among the practical advantages of optical stimulation over electrical stimulation, the optical method has minimal instrumental interference with simultaneous electrophysiological recording techniques. Furthermore, the method is technically scalable for accessing potentially multiple target areas for controllable spatiotemporal modulation across the cortex and deeper brain structures [9–12]. To advance such prospects, development of 'dual-function' chronically implanted devices for simultaneous light delivery and electrophysiological recording is needed. For localized light delivery, glass optical fibers have seen wide use in optogenetics to date, given their abundant commercial availability as flexible (though somewhat fragile) low-loss optical waveguides. In addition, an implanted optical fiber allows *in vivo* fluorescence detection in the intact brain for minimally invasive assessment of local opsin expression [13]. So far, recording of optically evoked neural activity *in vivo* for rodent and non-human primate models has been mainly limited to the use of individual extracellular electrodes which are adhesively attached in parallel to the optical fiber [12–16]. There are, of course, a variety of techniques in electrophysiology for neural population recording, ranging from multi-electrode arrays (intracortical and ECoG) to optical imaging [17–19], but these methods now need integration with fiber optics for chronic implants in the freely behaving animal experiments, which is the major motivation behind this paper.

Previously, we introduced an initial design and fabrication method of an optoelectronic device where an optical fiber was integrated to a 100 element ( $10 \times 10$ ) intracortical microelectrode array (MEA). This device was tested *in vitro*, to monitor neural activity in response to single site optical stimulation as a proof-of-concept application for triggering and mapping 2D epileptic wave propagation in optogenetically transduced mouse cortical slices [20]. Here we report an advance where a new version of this device, with a specially designed optical/electrical interface, was chronically implanted and tested in two rats, while being used for stimulation and recording in freely moving animals over 8 and 2 month experimental periods, respectively. The device enabled neuromodulation and simultaneous mapping of electrophysiological responses of neuronal populations in ChR2-expressing rats *in vivo*. We show below the use of

this device as an optogenetic tool for optical stimulation and electrical mapping of neural activity in a configuration which can be applied to other animal models.

## 2. Materials and methods

### 2.1. Integrated optrode-MEA device design and fabrication for chronic use

The design and fabrication of the integrated optrode-MEA device consisted of three steps: (a) the creation of a tapered optical waveguide used as a means of light delivery as a cortically embedded point source to optogenetically transduced targets, (b) the physical integration of such an optrode to the MEA and (c) means of affixing the integrated device to the head of the animal subject with suitable interconnects for tethered optical and electrical wiring to external instrumentation during experiments. The tapered optical fiber improved on design and fabrication which were recently reported as the single optrode [20] for *in vitro* focal light delivery and extracellular (single neuron) electrical recording (see figure 1(a)). This optrode, with or without the cladding metallic recording electrode layer exposed to brain tissue, was made specifically for chronic implantation in freely moving animals. The optrode elements were fabricated from a gold-coated step-index multimode optical fiber (50/125  $\mu\text{m}$  core/cladding with a custom-designed gold buffer, Fiberguide Industries). Gold buffer on both ends was carefully removed by mechanical stripping. Fiber tips were cleaved and cleaned with acetone and methanol before processing. The tapered end was created by standard wet etching in aqueous hydrofluoric acid (HF, 49%) at room temperature (22–24 °C). Tip taper angle (6°–30°) was controlled by the vertical pulling rate (0–20  $\mu\text{m} \cdot \text{min}^{-1}$ ). The tapered ends were shaped in such a way in order to minimize the neuronal damage during insertion. The distal end was connected to a custom-designed connector (Multimode SMA905, Thorlabs) and mechanically polished using polishing films (grit sizes of 3 and 1  $\mu\text{m}$ , Thorlabs). In those cases where the optrode was needed for electrophysiology as opposed to light delivery only, e.g. as a single self-standing device, the fiber was then rinsed in de-ionized water and loaded into a high vacuum thermal evaporator (Angstrom Engineering). A 25 nm thick titanium or chromium layer and 100 nm of gold film were sequentially deposited on the fiber (figure 1(b)). We found that the chromium layer enhances the adhesion between silica and gold film better than titanium. An electrical wire (magnet wire from Alpha Wire Company) was attached to the distal metalized part of the optrodes using silver epoxy (H20E, Epoxy Technology) and served as the conduit to external signal acquisition electronics. With the exception of the final 50–100  $\mu\text{m}$  of the tapered tip, the metalized part of the fibers was insulated using a UV-curable epoxy (Norland Optical Adhesive 81). Finally, the optrodes were encapsulated around the fiber connector by a heat shrink tube in order to prevent fracture and separation during possible bending. The scanning electron microscope image (figure 1(b)) shows the conductive coating covering most of optrode leaving only the very tip

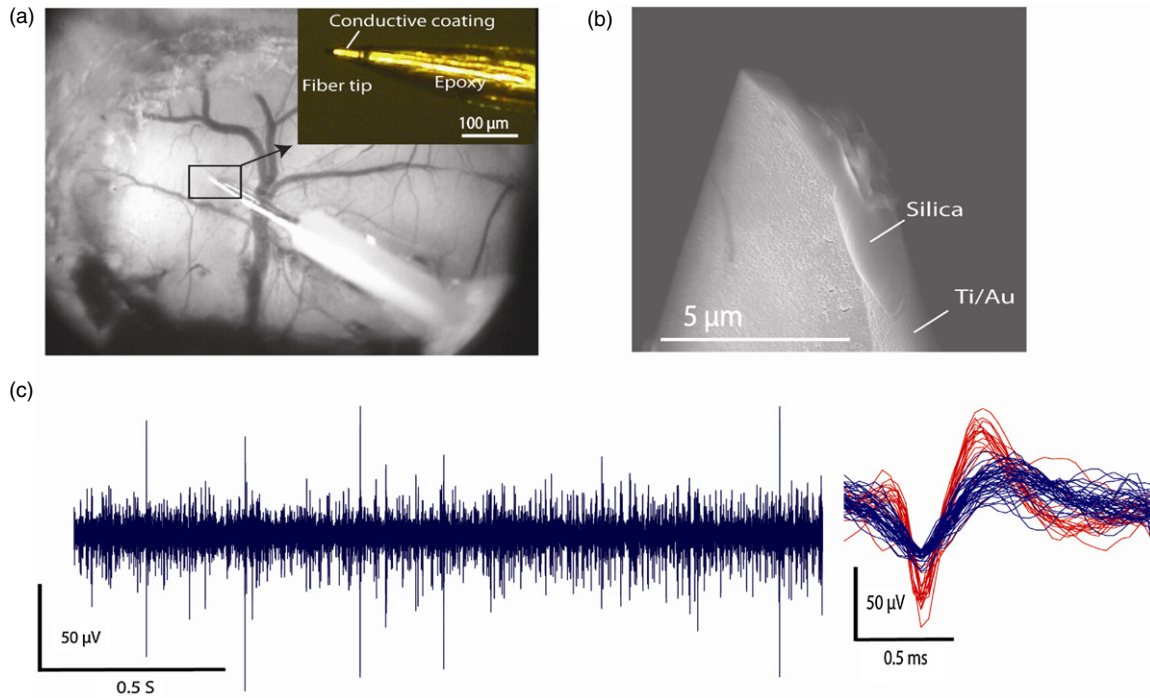


**Figure 1.** A single optrode as an *in vivo* electrophysiological recording tool. (a) Optical images of an optrode being slowly driven into the cerebellar cortex of an anesthetized mouse. The inset shows the detailed structure of the optrode. Light could be locally delivered through the aperture of the tapered optical fiber, while simultaneously the neural activities of nearby cells are recorded. (b) SEM image showing that the diameter of the optical aperture is about  $10\ \mu\text{m}$  in this optrode. The metal coating around the tapering tip, except the aperture, is indicated. (c) Examples of *in vivo* recording from an optrode. The left trace is the band pass filtered (300 Hz–10 kHz) recording of multiple unit activity from the cerebellar cortex of an anesthetized mouse as shown in (a). The  $V_{pp}$  noise amplitude was about  $30\ \mu\text{V}$ . The right panel shows the waveform samples from two isolated single units recorded by the optrode.

exposed for light delivery. The current version of the optrode is suitable for *in vivo* electrophysiological recording. The impedance values were within a range of  $200\ \text{k}\Omega$  to  $1\ \text{M}\Omega$ , enabling reliable detection of single- or multi-unit activities (figure 1(c)). An example of *in vivo* recording, measured with an extracellular recording amplifier (A-M Systems, Model 1800), from anesthetized mouse cerebellum is shown in figures 1(a) and (c). The optrode was mechanically strong enough to penetrate through the dura mater—an important design criteria for projected use in non-human primates.

In the next key fabrication step toward a chronic implant, the optrode (with or without recording capability) was integrated within a modified conventional multi-electrode intracortical array (figure 2(a)). We note that although the physical integration described next was important to fabricate and test the optrode-MEAs on a benchtop (with immersion to fluorescent dye-doped saline or agar), in the actual animal experiments, the sequence of integration was operationally different due to the intermediate steps of surgical implantation of the MEA, as well as the use of the laser drilled aperture for injection of optogenetic viral constructs (see section 2.2). The MEAs were based on commercial silicon-based electrode arrays, fabricated for our chronic rodent experiments as  $6 \times 6$  arrays of 1 mm long tapered Pt-tipped microelectrodes (Blackrock Microsystems) with an inter-electrode distance of  $400\ \mu\text{m}$ . The MEAs were further processed by ablative laser drilling to remove one silicon electrode at a chosen site (usually near the center), leaving a clear  $200\ \mu\text{m}$  diameter round hole in the structure. A Teflon cannula (C316GA,

Plastic 1) was centered with and bonded to the open hole on the backside of the MEA, with an approximately  $10\ \mu\text{m}$  tolerance. The function of the cannula was to provide a spatially stationary alignment guide for the viral injections and subsequent incorporation of the optrode as a light delivery tool for the chronic *in vivo* experiments. The integrated optrode-MEA construct in its final form is shown in figures 2(a) and (b). The design and the form factor of the single optrodes were chosen such that their shape and dimensions matched to those of the individual intracortical electrodes of the MEAs, though other fiber shapes are also possible, for minimizing tissue damage upon insertion into the cortex.

## 2.2. ChR2 transduction and optrode-MEA implantation

All procedures were conducted in accordance with the National Institutes of Health guidelines and approved by the Institutional Animal Care and Use Committee (IACUC) at Brown University. Subjects were two male Long-Evans rats (6–10 months, 300–320 g body weight), mildly food-deprived to 85% of free-feeding body weight and habituated to an operant chamber 2 weeks before the surgery. Surgeries were performed under aseptic conditions. The animals were anesthetized with 2% isoflurane–oxygen mixture, prepped, and placed in a stereotaxic apparatus (David Kopf Instruments). For one subject (M8), the craniotomy was centered on the posterior parietal cortex (PPC): anteroposterior (AP) =  $-4.5\ \text{mm}$  from bregma and lateral (ML) =  $4.5\ \text{mm}$  from the midline. The craniotomy was centered at



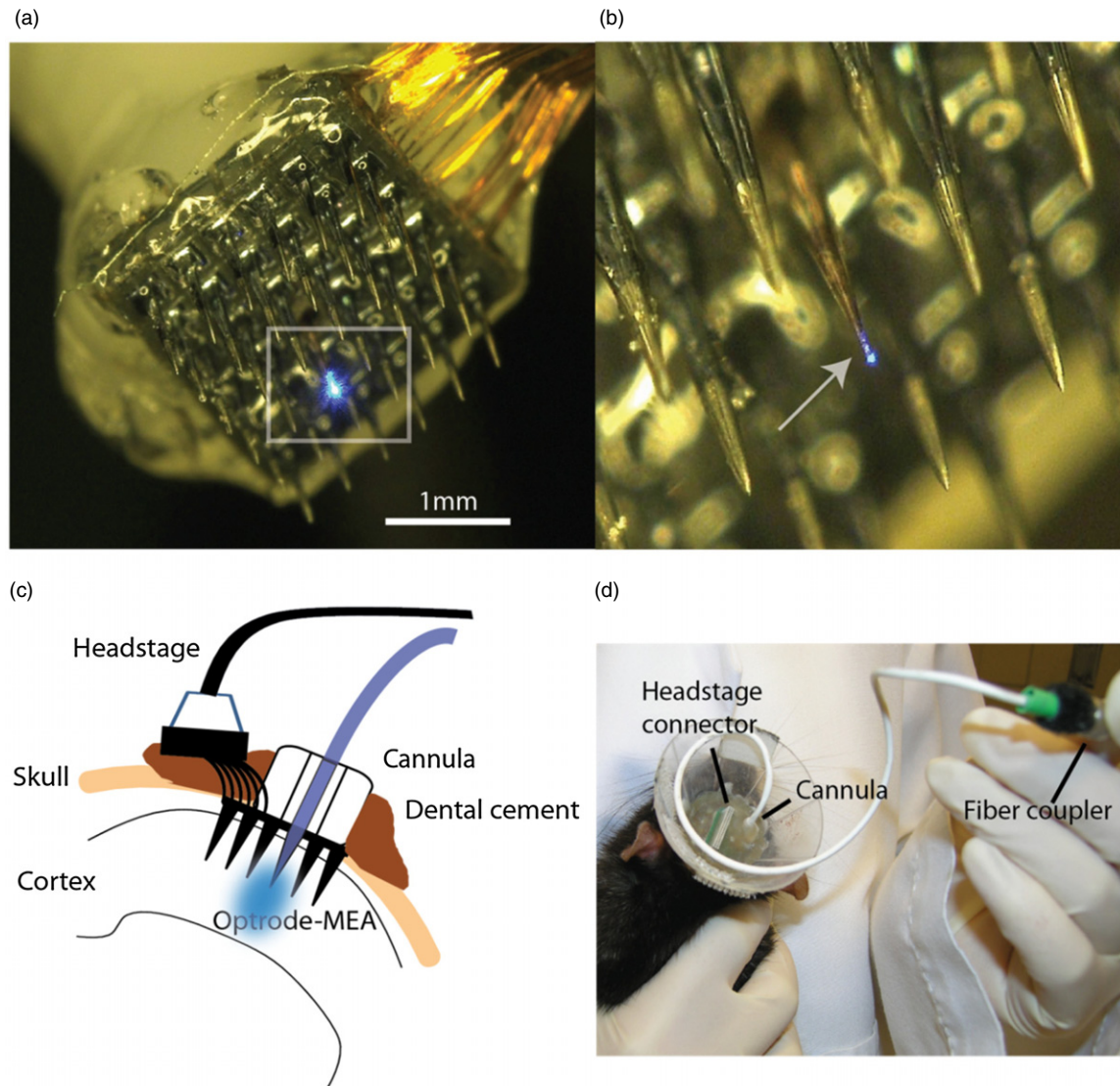


**Figure 2.** Overview of the optrode-MEA. (a) Image of the  $6 \times 6$  multi-electrode array device with one element being replaced by an optrode (arrow). The spacing between neighbor electrodes is  $400 \mu\text{m}$  and electrode shank length is 1 mm. (b) A close-up view of the optrode shows the laser light emitted from the tip of the optrode. (c) Schematic of the optrode-MEA implant, which shows the cannulated tube used to guide the optrode as well as the injection needle. (d) One of the subjects with the optrode-MEA implanted. The fiber optics and headstage connector are protected by a cone-shaped plastic cylinder. The optical fiber can be coiled and secured inside the cone after each recording session.

AP =  $-3.0 \text{ mm}$  and ML =  $2.5 \text{ mm}$  for the other animal (M9). Since the planar electrode array has dimensions of  $2.4 \times 2.4 \text{ mm}^2$ , it could cover sizable cortical areas, including the PPC, somatosensory cortex, and partially visual and association areas, on the right hemisphere. Prior to implantation, the MEA, optrodes and injection hypodermic needles were sterilized using ultraviolet light (hand held UV EF-160C, Spectroline) for 15 s to minimize the risk of infection. A series of holes were drilled for placement of six skull screws to provide mechanical support and a common ground reference was connected to two of them. A craniotomy window of  $3 \times 3 \text{ mm}^2$  was opened using a micro-drill (OmniDrill35 World Precision Instruments Inc.), mounted on the stereotaxic frame. The dura mater was carefully peeled away at the implant location to expose the cortex. The MEA (with its laser drilled hole and guide cannula) was

inserted slowly into the cortex ( $100 \mu\text{m} \cdot \text{min}^{-1}$ ) using a micromanipulator. This method of insertion caused less dimpling and bleeding of the brain compared to the impact insertion method [21] commonly used for this type of array. In addition, slow insertion allowed more precise control of the depth of the bare MEA in the brain. These all contributed to a higher success rate in obtaining chronic neural recordings. After insertion of about  $500 \mu\text{m}$ – $1 \text{ mm}$  into the cortex (including the slight brain swelling), the craniotomy was sealed with silicon elastomer (Kwik-Cast, World Precision Instruments Inc.) and the entire device was fixed in place using dental acrylic.

Viral injection for ChR2 transduction was conducted shortly after the acrylic was cured. A lentiviral vector was used to express ChR2 and a reporter fluorescent protein (EYFP) under the control of the human synapsin

promoter. Plasmid DNA encoding this transgene (pLenti-Synapsin-hChR2(H134R)-EYFP-WPRE, Optogenetics.org) was obtained from Stanford University and amplified using standard methods in molecular biology (MegaPrep, QIAGEN). VSV-G pseudo-typed lentivirus was produced at the University of Pennsylvania Vector Core. Typical viral titers were  $\sim 10^{10}$  IU mL<sup>-1</sup>. A convection driven injector with a hypodermic needle (G32 Hamilton) was slowly driven into the pre-defined cortical location through the guide cannula. Prior to actual injection, we advanced the needle beyond the target depth by 100  $\mu$ m and retracted it by the same distance to create a vacuous cavity. Column injection targeting at two depths (600  $\mu$ m and 900  $\mu$ m below cortical surface) was conducted by injecting the viral solution at a speed of 0.1  $\mu$ L  $\cdot$  min<sup>-1</sup> and volume of 1  $\mu$ L at each site.

Then, to complete the optrode-MEA integration during one and the same surgical procedure, the optrode element was gently held by a micromanipulator and inserted through the cannula guide. We ensured that the tip of the optrode was flush with the tips of the MEA electrode plane as pre-determined by calibrating the depth of insertion. Finally, the craniotomy was closed with silicone and acrylic. The connector for a compact headstage was mounted vertically atop the implant (figure 2(c)), and protected by a cone-shaped plastic cylinder (figure 2(d)).

### 2.3. Instrumentation for optical stimulation and electrophysiological recording by the optrode-MEA hybrid devices

The optrode fiber was coupled to a relay optical fiber using a standard fiber coupler. At the distal end, the relay fiber was coupled to a 473 nm blue solid-state laser (OptoEngine LLC) using a beam collimator (Thorlabs, FiberPort  $f = 4.6$  mm). Although there is 30% light loss at the interface between the optrode and relay fiber, we gained flexibility by using the miniature optrode and fiber connector. The laser was triggered by TTL pulses generated by a Matlab program via a digital I/O interface (NI USB-6501 National Instruments). The maximum optical power exiting the optrode optical aperture to the brain was measured to be 1.8 mW in the actual implant, sufficient to excite the ChR2-expressing neurons at the tip of the optrode, where the estimated average power density is about 916 mW  $\cdot$  mm<sup>-2</sup> (see sections 2.5 and 3.1.1). Time-stamp records of spikes, optical stimulus onset and behavioral events were saved digitally, as well as all sampled spike waveforms.

For electrophysiology, a miniature headstage amplifier (20 $\times$  gain) was used between the preamplifier module and the head-mounted connector. Signals passing through the preamplifier, which provides programmable gain and filtering (set at 150–8000 Hz band pass), were then recorded and processed by a Plexon Multichannel Acquisition Processor (Plexon Inc., Dallas, TX), a parallel processor capable of digitizing up to 32 channels simultaneously at 40 kHz rate [22]. Local field potential (LFP) signals of selected channels were also recorded with band pass filtering between 0.7 and 170 Hz and digitized at 1 kHz sampling rate.

### 2.4. Data analysis of the MEA recorded neural signals

Online waveform selection was performed by time-amplitude window discrimination [22]. Individual units were discriminated by employing principal component analysis or template methods (Offline sorter, Plexon Inc.). Further analysis employed commercial software (Nex software) and custom Matlab (MathWorks Inc.) programs. Peri-stimulus time histograms (PSTHs) were calculated with a bin size of 5 ms (except for determining the spike latency, where we used 1 ms bin), and the firing rate was defined as the trial-averaged spike counts divided by the bin size. Power spectrum analysis on the LFP was performed with a frequency range of 1–500 Hz and spectrograms were plotted with 1 s time shift window. The mean LFP power was defined as the integral of the squared LFP values over one period of light stimulation.

### 2.5. Light scattering in the brain: Monte Carlo simulation of photon propagation in tissue

Blue light (473 nm) is strongly scattered in neural tissue, placing limits on the activation volume of ChR2-expressing brain tissue emanating from an ideal point source as opposed to the actual absorption by ChR2-transduced neurons at a given cortical target site. We implemented a computational model to estimate the intensity at various locations from the light source, i.e. the optrode. We performed a Monte Carlo simulation that treats the brain tissue as a heterogeneous scattering and absorptive medium as described in Yaroslavsky *et al* [24]. Accordingly, we employed an anisotropic scattering model based on the Henyey–Greenstein phase function (equation (1)) [23]:

$$p(\cos \theta) = \frac{1 - g^2}{(1 + g^2 - 2g \cos \theta)^{3/2}}. \quad (1)$$

This function gives a model distribution of the direction change of scattered photons.  $\theta$  is the polar angle in the spherical coordinates. Conventionally,  $p(\cos \theta) d\theta$  expresses the probability of direction change falling into the range  $\theta \rightarrow \theta + d\theta$ . The anisotropy factor  $g \in [0, 1]$  indicates the spatial uniformity of the scattering, with  $g = 0$  being no preference to any direction and  $g = 1$  being mostly forward scattering. We employed an anisotropy factor of  $g = 0.88$  in our simulation. The scattering and absorption coefficients used were 10 and 0.07 mm<sup>-1</sup>, respectively, for blue light as obtained from the diffuse reflectance and transmittance measurements of human brain tissue [24]. Therefore, the brain tissue was considered as a continuum of scatterers and absorbers distributed uniformly.

In our optrode-MEA device, light traveling down to the optrode is strongly confined by tapered fiber optics and its (optional) metal coating. To simplify the model, we treated the optrode as a point light source with a given initial beam divergence, while placing it in the center of a cube with dimensions of 2  $\times$  2  $\times$  2 mm<sup>3</sup>. The cubic region of interest was divided into 200  $\times$  200  $\times$  200 volume differential elements (voxels), so that voxel spatial resolution (10  $\mu$ m, approximately one tenth of the mean free path of a photon

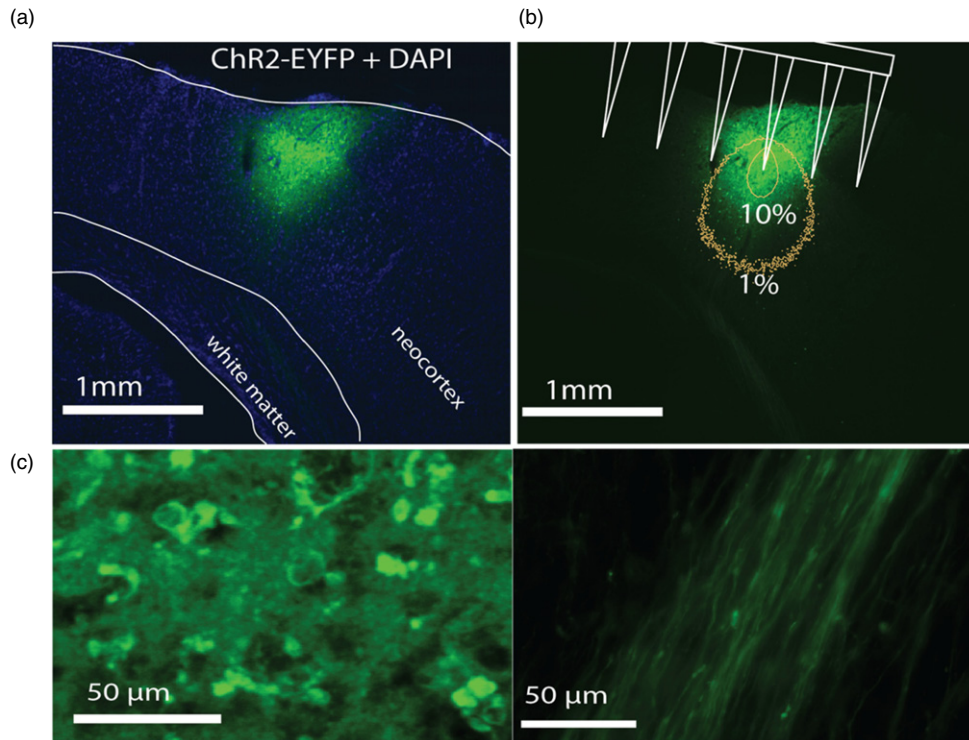


**Figure 3.** The Chr2-expressing volume and the optical excitation volume. (a) A fluorescence image of a coronal slice that resolves individual EYFP-opsin expressing neurons. The cell nuclei were indicated by DAPI staining. (b) The Monte Carlo simulation of the photon count (proportional to light intensity) distribution in brain tissue. The contours of 10% and 1% of the iso-intensity are indicated by yellow dots. The light intensity reaching the neighbor electrodes is  $5 \text{ mW} \cdot \text{mm}^{-2}$  estimated from the simulation (see details in the text). The output light from the optrode is approximated as a point source and has a divergent angle of  $30^\circ$ . (c) The enlarged images display cell bodies (left) and fibers (right) that project to subcortical structures.

traveling in brain tissue) was sufficient to map the distribution of the light intensity. A packet of  $10^6$  photons was launched from the source, uniformly distributed according to a chosen angle of divergence. The maximum divergence angle chosen was  $30^\circ$  to the  $z$ -axis of the fiber, acquired from a separate experimental observation we made for the emission profile of the optrode immersed and imaged in a control fluorescent dye solution.

Figure 3(b) shows the results of the simulation, a cross-sectional image of photon density (proportional to light intensity) in the  $x$ - $z$  plane, in relation to the optrode source and adjacent microelectrodes of the MEA. The simulation of light distribution in brain tissue was in good agreement with photoimaging experiments, which we performed *in vitro* in the slice preparation (data not shown), except in the immediate vicinity of the optrode (within one mean free path for photons to the point source). We note that, while alternative models for numerical solving of the photon diffusion equation exist, they are generally considered less accurate near the light source due to the invalid approximations made at this region [25]. We return to the utility of these numerical simulation results below in section 3.

### 2.6. Histology and fluorescence imaging

At the conclusion of the experiments, subjects were deeply anesthetized with pentobarbital sodium (Beuthanasia-D) and transcardially perfused. Brains were fixed in 4%

paraformaldehyde for 4 days and then equilibrated in 28% sucrose in PBS.  $40 \mu\text{m}$  thick sections were prepared with a freezing microtome and stored in PBS at  $4^\circ\text{C}$ . DAPI staining (1:15 000) was conducted following standard immunohistochemical procedures. Sections were mounted on glass slides, and sealed by the mounting medium (VECTASHIELD, Vector Laboratories, Inc.) to prevent rapid loss of fluorescence during microscopic examination. Confocal fluorescence images were acquired with a microscope (LSM510, Carl Zeiss) using the  $5\times$  and  $63\times$  (oil-immersion) objectives. Nissl body staining (in a 0.1% cresyl violet solution) was performed on the two subjects (M9 and M8) implanted for 2 and 8 months, respectively. The Nissl stain images were acquired using an optical microscope. Images were further analyzed and processed using two software packages (ImageJ and Adobe Illustrator). The images are shown in figures 3 and 7, and commented on further below.

## 3. Results

### 3.1. Observation and characterization of *in vivo* neuromodulation via optogenetic activation in freely moving rats

In this section we describe results from chronic implant experiments, with the aim of demonstrating that now the optrode-MEA device can be used for *in vivo*, freely moving



rodents to map spatiotemporal patterns of the optically induced neuromodulation in the cortical area defined by the microelectrode reach of the MEA. We place less emphasis in this paper on the recording of the single optrode itself, i.e. at the very point of light delivery, since this is a complex topic, including the possible light-induced damage to neurons in the immediate zone at the end of the optrode tip. Likewise, there are ongoing investigations which aim to study possible photoinduced detrimental effects to the cells in the immediate vicinity of the small aperture tip during long term light exposure in chronic applications.

**3.1.1. ChR2 expression and optical stimulation pattern of the optrode in the rat brain.** For each animal, we began the optical stimulation and neural recording session from about 2 weeks after initial viral injections, so as to allow reasonable time for ChR2 expression to develop. As an empirical measure of the level of ChR2 expression, we employed the amplitude of light-induced LFP. We found that light-induced responses ramped up to their maximal amplitude in about 4 weeks after injection and persisted at a relatively stable level in the following 2–4 weeks. This observation agrees with those reported recently via *in vivo* tracking of fluorescence protein expression by a fiber optics opsin detector [13].

At the end of experiments, animals were perfused and brains sectioned for immunohistochemistry to (a) visualize the location and transduction efficiency of ChR2 expression and (b) examine the anatomical imprints of the chronic intracortical arrays. Most importantly, the center of injection site showed strong expression as indicated by fluorescence from co-expressed EYFP in the fusion plasmid. Confocal microscope images, co-labeling with YFP (opsin marker) and DAPI (nuclear marker), are shown in figure 3(a). The estimated spread of ChR2 was 700  $\mu\text{m}$  in the horizontal direction and 1 mm in the vertical plane as indicated in this particular brain section. The human synapsin promoter, which exclusively targets neurons, resulted in strong expression of the opsin in cell bodies, processes as well as fibers that project to subcortical structures (see figure 3(c)) [13].

Conventionally, the methodology for *in vivo* optogenetic stimulation and neural recording uses an optical fiber mechanically attached to an electrode [26]. Therefore the distance between recording and stimulation sites is predefined and it can only sample one recording site at a time. Another commercially available optrode recording unit (NeuroNexus) combines the multi-shank silicon probes with a bare optical fiber [9, 27]. The loose confinement of the etched waveguide might cause the problem of low spatial resolution, as discussed in [9]. The principal advantage of the optrode-MEA hybrid device lies in its capability to optically modulate at one site (or with more than one fiber, at multi-sites) while recording extracellularly from an ensemble of those neurons that define the microcircuitry environment in the vicinity of the stimulus site. One important aspect of this approach is the ability to control the size of excited brain volume by controlling the emitted optical power and its distribution within the brain. In free space, the point source optical output from the optrode tip spreads with a divergence angle of  $30^\circ$ . This conical emission,

if preserved, would target only a confined region of brain tissue within a conical volume below the optrode tip. The power density of the emission cone would drop approximately with the inverse of the square distance between targeting neurons and optrode tip. However, the laser wavelength (473 nm) optimized for ChR2 excitation is strongly scattered, and weakly absorbed in neural tissue. These properties of the tissue are expected to have significant effects on the spatial distribution of light power.

As described above in section 2.5, to enable the estimation of the volume of light-induced ChR2 activation in the cortex with the tapered fiber, we implemented a Monte Carlo model, to calculate the spatial distribution of light intensity at various locations around a point source with an emission divergence angle of  $30^\circ$ , as an approximation to the optrode tip (see section 2). Returning to figure 3(b), the numerical simulations show the 10% and 1% contours of iso-density of photons (proportional to light intensity) as a cross-sectional image in the  $x$ - $z$  plane, positioned relatively close to the light source and adjacent to microelectrodes of the MEA. The simulations for the taper in question showed how the iso-intensity plane from the hypothetical optrode becomes oval shaped at 300  $\mu\text{m}$  (about three times the photon mean free path length for scattering events) away from the tip. According to previous *in vitro* and *in vivo* works [7, 16], the minimal light intensity required for spiking of ChR2-transduced neurons is on the order of  $1 \text{ mW} \cdot \text{mm}^{-2}$ . Under our stimulus parameters (1.8 mW power at the optrode tip), the light intensity is estimated to be  $5 \text{ mW} \cdot \text{mm}^{-2}$  at the site 400  $\mu\text{m}$  lateral to the stimulus, enough to activate ChR2-expressing cells around the neighbor electrodes. Therefore, the optrode was able to deliver a more than adequate level of light for optogenetic excitation to a volume whose size is primarily determined by tissue scattering and the power output at the tip of the optrode. (We note that high optical intensities do, however, exist near the tip aperture, though considerably less e.g. than typically employed in two-photon microscopy.)

These results indicate that the total volume of excitation through the optrode was determined mainly by the optical power distribution in the brain rather than the expression volume of ChR2. In addition, our optrode-MEA device covered a larger area than both the ChR2-expressing region and the optical distribution, thereby making it possible to monitor the spread of activity in a network of neurons in response to local stimulation.

### 3.2. Observation and characterization of *in vivo* neuromodulation via optogenetic activation in freely moving rats

In this section we demonstrate the performance of the optrode-MEA hybrid device through selected examples of its utility of operation in freely moving rats, with a focus on recording and mapping the optically induced modulation of neural activity across the  $2.4 \times 2.4 \text{ mm}^2$  cortical area spanned by the planar MEA.



**3.2.1. Optical neuromodulation of single-unit and LFP activity.** In optogenetics, targeted cortical illumination can modify spiking activity in many neurons, as well as LFPs, which were here monitored across the MEA recording sites. Figure 4(a) displays an example of one light-responsive neuron in animal M8, including raster plots of the spikes, their firing rates from PSTHs, as well as trial-averaged LFPs. Each light train lasted 5 s with peak intensity of  $5 \text{ mW} \cdot \text{mm}^{-2}$  at the specific MEA electrode as estimated by our Monte Carlo simulation. The blue marks indicate the individual pulses of 20 ms duration. For example, a neuron could reliably respond to the stimulation with an approximately three-fold induced increase in the probability of spiking (figure 4(a) top), while the spike waveform shape remained unaltered. The lowest trace of figure 4(a) represents the trial-averaged LFP, recorded at the same site, in response to pulse train stimulation. The evoked LFP showed a negative deflection followed by a small positive rebound, in accordance with the expected current flow. Since the proximal MEA electrodes were close to the excitatory Chr2-expressing volume, this type of LFP behavior thus reflected the inward ion flow due to excitation in this area (i.e. near the current sinks) at the initial phase of LFP response.

We further used the simultaneously measured LFPs in animal M8 while asking the question whether optical excitation might be able to induce a collective response of neuronal ensembles in response to the pulsed stimulation at specific repetition rates (frequencies). The extracted power spectrogram (figure 4(b) left) demonstrates the enhanced activity at the stimulation frequency and its harmonics. Investigating the strength of neural activity at varying stimulation frequencies could in principle give another dimension of information about how the neural network responds to optogenetic stimulation. Figure 4(c) illustrates the LFP power as a function of light intensity at the recording electrode. The variation of LFP power was calculated based on recordings from ten sequential pulse trains with the same stimulation parameters. The actual output power variation at the optrode tip was measured in an *in vitro* setting by intentionally bending or twisting the fiber optics and the range of power densities at the recorded site (the horizontal error bars shown in figure 4(c)) was then obtained from the Monte Carlo simulation. This was meant to give a measure of variability of output intensity due to animal movement. The approximately linear relationship between LFP power and light power indicates that we were not obviously ‘over-driving’ the neural network by saturating the optical stimulation response. The high degree of repeatability of the responses allowed us to drive stimulation rates up to 30 Hz for a synchronous response (data not shown here), which suggests how the optrode-MEA could be a useful tool for activating and probing the collective neural network behavior such as rhythmicity across cortical areas of specific interest.

**3.2.2. Comments on photoinduced artifacts and use of controls for validating stimulation.** One caution raised by the combination of optical stimulation and simultaneous electrical recording is that the light stimulus can induce

electrical artifacts [28]. Even if much less of a hindrance than the interference which is always present in the case of recording during direct electrical stimulation [29, 30], optical artifacts are caused by direct photoelectronic or photoinduced temperature effects depending on the optoelectronic properties of materials at the recording interface. We have found it convenient both to quantitatively calibrate as well as to discriminate against such finite artifacts, e.g. from field potentials, by carrying out separate control measurements in the cortex of a freshly sacrificed animal. An example of optical artifacts (top trace labeled ‘Control’ in figure 4(d)) was recorded from an electrode in the MEA  $\approx 0.57 \text{ mm}$  away from the optrode. We see a fast recovery ( $< 5 \text{ ms}$ ) to the small, if finite, effect, whereas the actual LFP response in the rat’s brain (lower black trace) has a much slower effect ( $\sim 50 \text{ ms}$ ) elicited by the light stimulus. We also used a simple ‘brain phantom’ made from 2.5% by weight of agarose in a saline solution to emulate and quantify the optical artifact as well as light scattering properties of brain tissue. We obtained similar results with the ‘brain phantom’ (data not shown here) as with the control brain tissue. As another control, we also tested the neuromodulation of single units and population *in vivo* by stimulating with yellow light (561 nm, and same parameters as the blue excitation light). Due to the finite absorption tail of the Chr2 chromophore (retinal) at this wavelength, we did observe a finite response, but with LFP amplitude that was decreased to 19% of that using blue light stimulus (data not shown here).

### 3.3. Mapping of ensemble neuronal activity across cortical areas in rats by the optrode-MEA device

As another example of illustrating how we used the optrode-MEA to acquire real-time spatiotemporal maps of the neural response across a finite population of neurons, figures 5 and 6 show sample results from animal M9, where the implant was now centered at the somatosensory cortex, with the stimulus and recording taking place at a depth of approximately 1 mm. To further demonstrate the ability of our dual function device to monitor multiple units and collective neural activity in response to local optical neuromodulation, figure 5(a) shows an illustration of the ‘topographical’ mapping of waveforms of 17 isolated units acquired within a recording session from animal M9. In order to discriminate the firing behavior of neurons in figure 5(a), we demonstrated the modulated firing rates of single units as a function of their distance from the site of optrode stimulation, as shown in the scatter plot of figure 5(b). Each dot in figure 5(b) indicates the fraction of the firing rate change for an individual unit, which is defined as

$$\text{Fractional change} = \frac{\text{FR}_{\text{stimulated}} - \text{FR}_{\text{baseline}}}{\text{FR}_{\text{baseline}}}$$

A paired *t*-test was performed on the firing rates of the baseline epochs (500 ms period before stimulus) and that of stimulation epochs. Most recorded neurons changed their firing rate significantly in response to stimulus as indicated by the filled dots in figure 5(b) ( $p < 0.05$ ). In addition, neurons within 600  $\mu\text{m}$  of the optrode, i.e. those recorded from the nearest

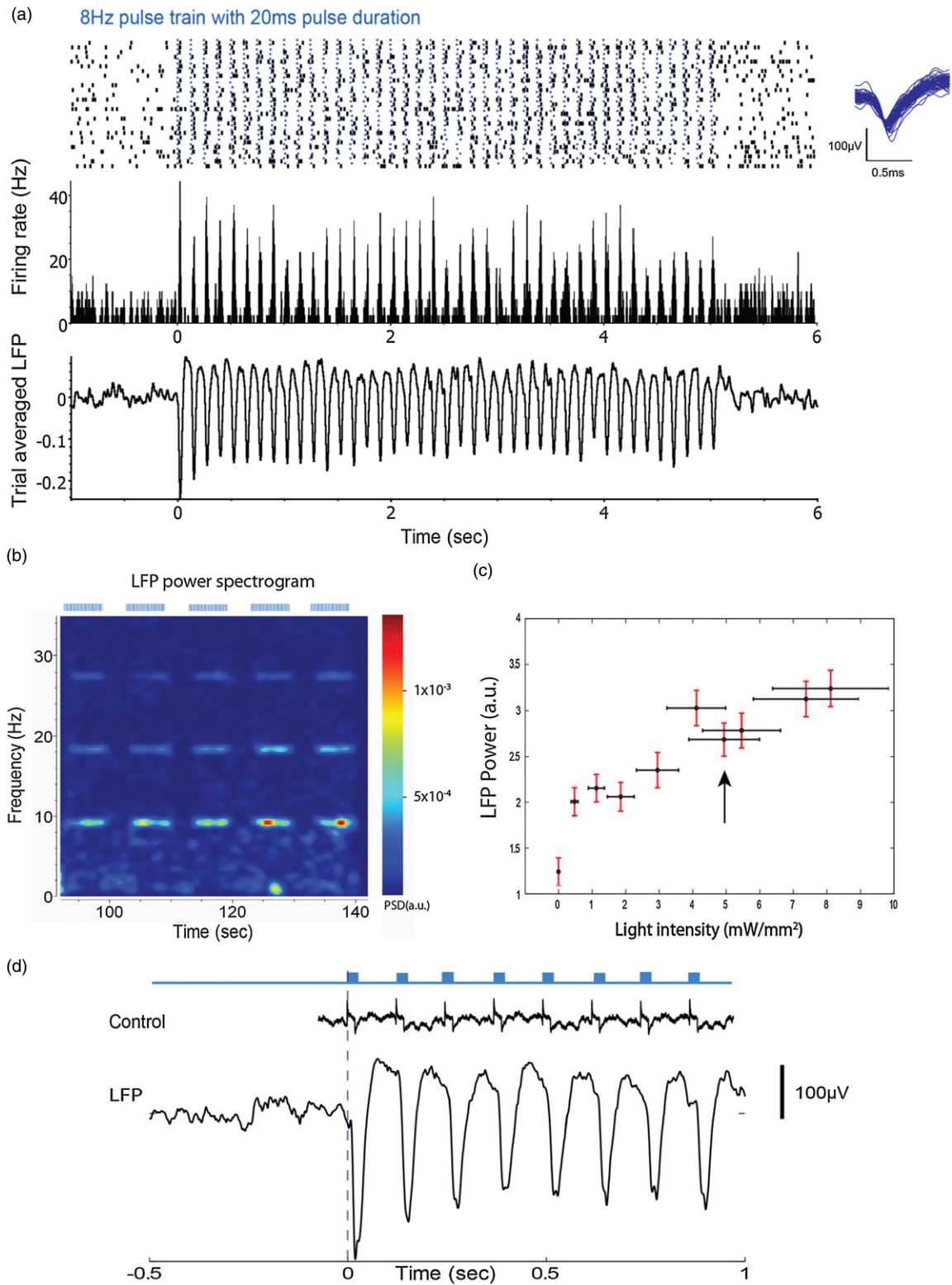


**Figure 4.** Representative examples of light activation of single units and LFPs. (a) Raster plots and PSTHs from a light-responsive cell after 5 months of implantation. The blue tick indicates the pulse train stimulation (473 nm, 8 Hz pulse frequency and 20 ms pulse duration). A sample of overlaid spike waveforms is shown on the right. The lower panel shows that trial-averaged LFP has negative deflections with a positive rebound in response to each pulse stimulation. (b) Power spectrogram and power density plot of optically modulated LFP. Note that the power is significantly enhanced at the light stimulation frequency and its harmonics. (c) LFP power around the pulse stimulation frequency as a function of estimated light intensity at the recording electrode site (see the text for details). The arrow indicates the light intensity used for neural stimulation in the rest of the paper. (d) Optically induced LFP response and comparison with control recordings. ‘De-sensitization’ is shown as the amplitude of negative peak decreases in response to repeated optical stimulation.

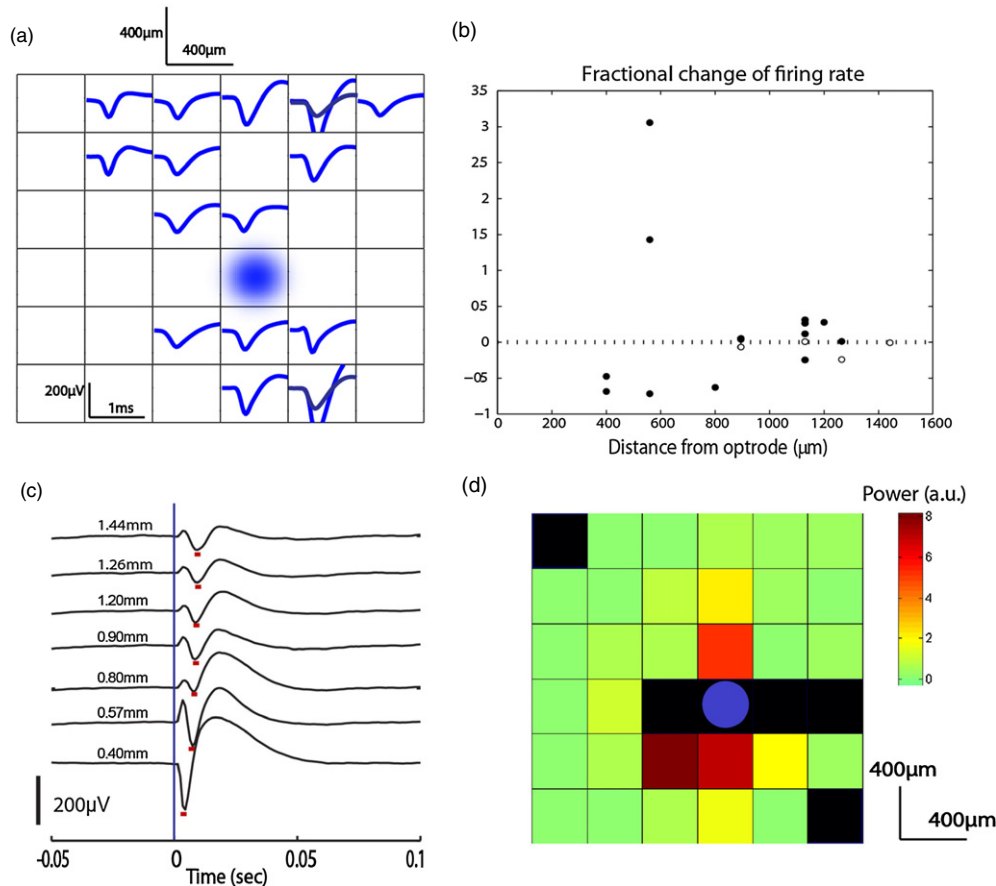


**Figure 5.** Spatially and temporally resolved neuronal activities from a large cortical area. (a) The mapping of averaged ( $N = 100$ ) spike waveforms on each input channel obtained from a sample recording session. (b) The fractional change of firing rate (see details in the text) of single units as a function of the distance between the recording electrode and stimulating optrode. The firing rate data were collected from the same set of isolated units as in (a). (c) Pulse-triggered LFPs at various locations show both proximal and distal field potential in response to the 1 ms pulse stimulation. The vertical line indicates the onset of light pulse and red dots indicate the negative peaks. The output power of the optrode is estimated to be 1.2 mW. The distances between the recording electrode and the optrode are labeled on the individual traces. (d) Mapping the full-band power of pulse-triggered LFP over  $2.4 \times 2.4 \text{ mm}^2$  cortical area. The black color indicates the sites without recordings. All PSTH and LFP signals shown in figure 4 are averaged over 30 trials.

and next nearest electrodes, had larger fractional change in their firing rate than those further away from the stimulation site ( $p < 0.01$ ).

The optrode-MEA device was able to consistently monitor on average  $13 \pm 5$  isolated units at each recording session. However, the recording sites, and probably the recorded units, varied from session to session. Claims that the same neurons are recorded necessarily assume some metrics based on, for instance, waveform shapes and inter-spike interval histograms. However, each of these measures can be subject to controversy. In one of the comprehensive studies on this issue, the authors estimated that about 39% of single units were stable across 15 days in their primate recordings [31]. Comparing such an epi-cortical ‘floating’ MEA with our skull-anchored optrode-MEA, we expect that the chance of stable recording from the same units would be less in the latter case. A similar systematic study in the rodent model is beyond the scope of this present work which aimed at a proof-of-concept device demonstration, but we note that in future planned deployment of the optrode-MEAs in primates, skull mounting of the devices is unlikely to be used due to larger anatomical workspace.

The capability of recording whole bandwidth signals, spikes and LFPs with high spatiotemporal precision gives us the opportunity to study the dynamics of neuromodulation by light by concentrating on specific spectral power bands. Focusing next on LFPs, we recall that spatial mapping of LFPs enables tracking of the propagation of activity through the network at a more global level. Therefore, the optrode-MEA hybrid device offers the opportunity to study the dynamics of networks affected by neuromodulation via LFP recordings. To explore this aim for animal M9, we plot the averaged LFPs, aligned to the onset of 1 ms stimulus light pulse (the vertical line shown in figure 5(c)), recorded from various locations at the top-left corner of the device (refer to figure 5(d) for ease of visualization). The ‘void’ channels, indicated by black in figure 5(d), were due to the laser drilled hole and wiring configuration of our current recording system. A video clip of the same data showing the dynamics of LFP activity is available in the supplementary materials available at [stacks.iop.org/JNE/9/016001/mmedia](http://stacks.iop.org/JNE/9/016001/mmedia). All PSTH and LFP signals discussed above represent averages over 30 trials. Interestingly, the data show quite different activation profiles

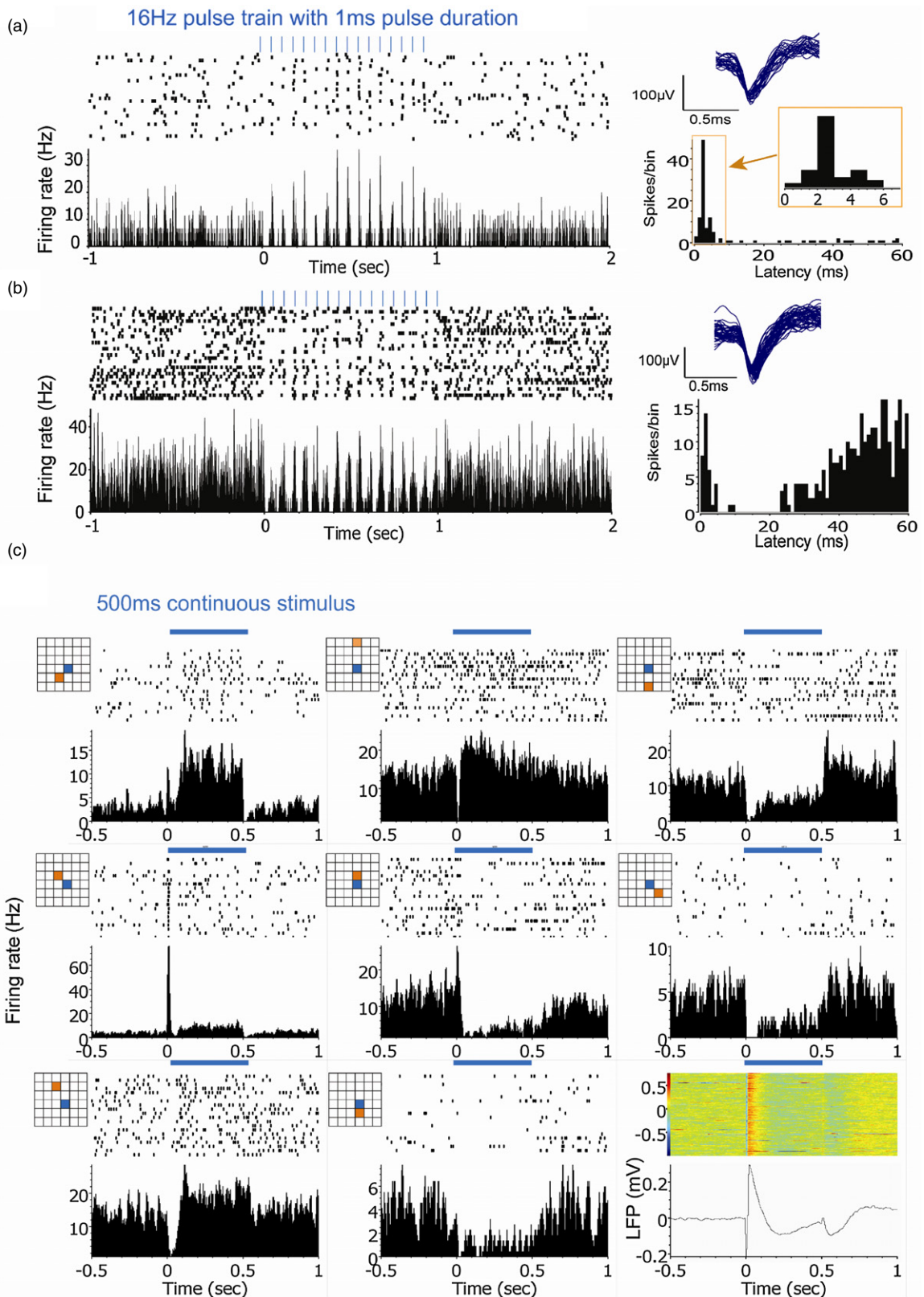


**Figure 6.** Examples of single-unit recordings under light modulation. (a) Raster plots and PSTHs from a neuron activated by the pulse train (blue ticks). The spike count histogram (right panel) shows the time-locked spikes evoked by the stimulation. Samples of selected spike waveforms are plotted on the right. (b) A unit showing an inhibitory response to the same stimulation. (c) Examples of activation patterns of single units at selected sites across the MEA (insets indicate locations), in response to 500 ms continuous light stimulation. The last plot is an example of LFP response.



for proximal and distal fields in response to the light stimulus. The ‘nearest neighbor’ electrode, 400  $\mu\text{m}$  away from the excitation spot, has a rapid negative deflection followed by a slow positive rebound, whereas distal electrodes demonstrate opposite polarity at the beginning and shifted peak (red dots) according to their distance from the optrode. A more detailed current source density analysis of these types of LFP recordings by multi-electrode arrays should allow for more accurate identification of current sinks and sources over space and time [32]. However, in this work we were limited by the 400  $\mu\text{m}$  fixed-grid spacing between MEA electrodes as well as the limited number of available LFP recording sites to conduct such an in-depth analysis.

### 3.4. Cell-type diversity suggested by the variability observed in the neuromodulatory circuit response to optical stimulation

We now comment on our observations where pronounced variation has been seen in the nature and magnitude of the modulated electrophysiological responses across a population of single units. To first order, these MEA accessible (excitatory and inhibitory) neurons can be assumed to be a mixture of those cells which can be directly modulated by light and those which lie outside the optrode excitation ‘field of view’ (given the estimated light emission pattern of e.g. figure 3(b)). The latter population is then likely to be only indirectly modulated by the blue laser excitation, reporting via a local network effect triggered from within the photoexcitation volume ( $\sim 1 \text{ mm}^3$ ). Consider first a given cell and its direct modulated responses to the 1 ms light pulses shown in figure 6(a), resulting in an increase in the instantaneous firing rate as shown in the PSTH data in the figure. The pulse-triggered average of spike delay, plotted as latency in the right-hand inset of figure 6(a), shows well-defined, time-locked spiking with 3 ms delay following the blue light pulses, which is an indicator of direct channel activation. Here, we defined a ‘direct zone’ amongst the recording electrodes that are within 0.57 mm of the stimulation center. We have seldom encountered such directly activated units outside the optrode ‘field of view’, which is also consistent with the distances from Monte Carlo light scattering/absorption simulation results as well as the somewhat larger Chr2-expressing volume acquired deduced from later histological studies. As for variability, we show by contrast another neuron, depicted in figure 6(b), which displayed light-induced responses, but now with a ‘silent’ period for about 30 ms after light pulse, probably caused by an indirect-pathway inhibitory input from Chr2-expressing neurons.

Finally, we also employed continuous stimulation, whereupon the blue laser was constantly on for the entire period of 500 ms. Using this condition as a case example, we show in figure 6(c) the time-resolved mapping of the neural response from multiple sites across the MEA from a sample recording. The images demonstrate various patterns of modulated single-unit activities in terms of the light-triggered raster plots of spiking and their PSTHs in the individual panels, with the relative locations of the MEA electrodes to the stimulus site indicated by the accompanying insets.

The diversity of responses exemplified above illustrates the intricate dynamics of the photomodulated cortical network. Some cells were tonically excited or inhibited throughout optical stimulation, whereas other neurons showed a phasic response followed by a more sustained activity. For example, the cell on the second row, first column (figure 6(c)) increased its firing rate for a few milliseconds after the onset of light stimulation, before going back to its baseline firing rate. Another cell (first row, second column shown in figure 6(c)) was first inhibited and then increased its firing rate above baseline for the rest of the stimulation. The observed variety of responses is likely due to a sequence of direct and indirect (synaptic) optical modulation of activity. In these first chronic experiments, the animals were not subject to any trained task so that no explicit correlation with behavior was investigated; rather the emphasis here is to underscore the potential utility of the optrode-MEA device for mapping optically modulated activity. Experiments that connect with specific training paradigms are under way.

### 3.5. The chronic optrode-MEA implant and possible tissue damage

As an indicator of the impact of the chronic implant of the optrode-MEA devices on cortical tissue, figure 7 shows examples of two cases of Nissl stained slices from two subjects after 2 and 8 months of duration. No apparent behavioral changes were observed in either subject during these time periods during their recording sessions or in home cages, respectively. We did not find any obvious signatures of tissue/array interaction, which was consistent with stable recording extracellularly from single units over months by standard MEAs as shown in many experiments in non-human primates [33]; however, clear traces of microelectrode/optrode tracks can be seen in figure 7(a), not unlike in chronic monkey experiments with the very same types of MEAs [34]. In the present case, the effects of possible additional light-induced damage in contributing to the ‘mechanical’ damage remained unclear. Rather, a significant depression of the cortex is present in the images, suggesting that improvements must be made in future experiments with the approach of flexibly anchoring the optrode/MEA devices in rodent use. We believe that the cortical depression is not caused by the arrays themselves *per se* (even if their footprint for a rodent is smaller than the approximately  $4 \times 4 \text{ mm}^2$  area of the 100 element MEAs for primates), but rather the rigid way that the arrays were anchored to the animal skull in these first experiments in freely moving rodents.

## 4. Summary

We have developed an intracortical device for simultaneous *in vivo* optical stimulation and multi-site extracellular recording which integrates a single localized custom-designed and fabricated optrode into a commercially available MEA. We described above the device design, fabrication and its surgical implantation into rats. The experiments demonstrate the capability to measure optogenetically mediated neural

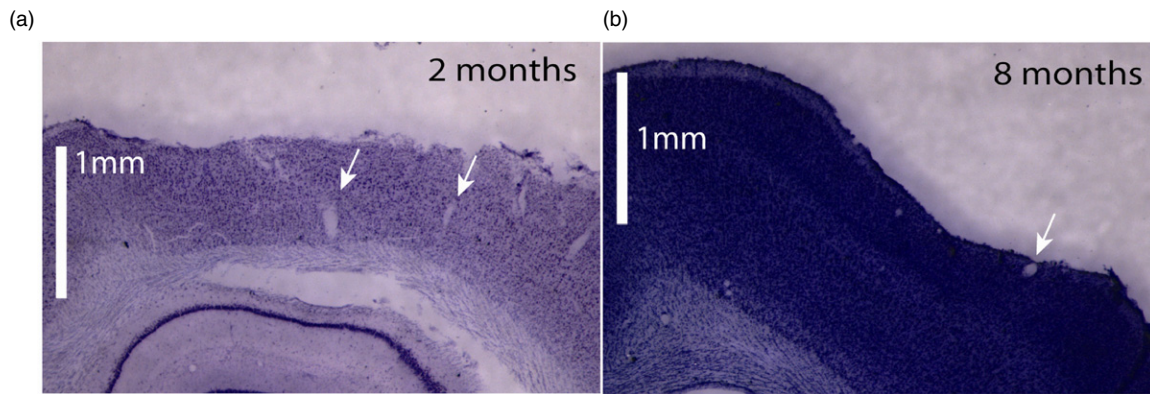


**Figure 7.** Results from histology studies. Nissl staining shows the anatomical impact of the chronic optrode-MEA devices after implantation. Cortical depression of approximately  $100\ \mu\text{m}$  was observed in (a) one subject 2 months after surgery, and about  $350\ \mu\text{m}$  depression was observed in (b) another subject 8 months post-implant. The arrows point to the clearly identifiable traces of individual microelectrodes and the optrode.

stimulation in freely moving animals over periods of months. While we have emphasized the device engineering in this paper, we believe that the device construct described above can lead to extraction of new scientific information about neural microcircuit dynamics under *in vivo* optical stimulation such that optical neuromodulation can be combined with both population recording and neural signal decoding, in the context of specific behaviors and tasks. Short term applications of this device can include investigating basic network properties and characterizing the propagation of activity throughout this network at a spatial scale intermediary between intracellular recordings and ECoG or EEG recordings such as those of importance, for example, in the study of epilepsy [35]. This optrode-MEA device has been designed to be scalable for accommodating additional optrode sites to enable spatiotemporal patterned light activation or inhibition for targeting specific cortical regions or subcortical structures.

## Acknowledgments

This work was supported by the Defense Advanced Research Projects Agency (Repair Program) contract N66001-10-C-2010, and the National Science Foundation EFRI program grant 0937848. We thank Dr Leigh Hochberg for useful discussion and Dr Jonathan Ho for helping prepare the brain sections.

## References

- [1] Histed M H, Bonin V and Reid R C 2009 Direct activation of sparse, distributed populations of cortical neurons by electrical microstimulation *Neuron* **63** 508–22
- [2] Nagel G, Szellas T, Huhn W, Kateriya S, Adeishvili N, Berthold P, Ollig D, Hegemann P and Bamberg E 2003 Channelrhodopsin-2, a directly light-gated cation-selective membrane channel *Proc. Natl Acad. Sci. USA* **100** 13940–5
- [3] Schobert B and Lanyi J K 1982 Halorhodopsin is a light-driven chloride pump *J. Biol. Chem.* **257** 10306–13
- [4] Chow B Y et al 2010 High-performance genetically targetable optical neural silencing by light-driven proton pumps *Nature* **463** 98–102
- [5] Deisseroth K, Feng G, Majewska A K, Miesenböck G, Ting A and Schnitzer M J 2006 Next-generation optical technologies for illuminating genetically targeted brain circuits *J. Neurosci.* **26** 10380–6
- [6] Zhang F et al 2007 Multimodal fast optical interrogation of neural circuitry *Nature* **446** 633–9
- [7] Boyden E S, Zhang F, Bamberg E, Nagel G and Deisseroth K 2005 Millisecond-timescale, genetically targeted optical control of neural activity *Nat. Neurosci.* **8** 1263–8
- [8] Zhang F, Aravanis A M, Adamantidis A, de Lecea L and Deisseroth K 2007 Circuit-breakers: optical technologies for probing neural signals and systems *Nat. Rev. Neurosci.* **8** 577–81
- [9] Royer S, Zemelman B V, Barbic M, Losonczy A, Buzsáki G and Magee J C 2010 Multi-array silicon probes with integrated optical fibers: light-assisted perturbation and recording of local neural circuits in the behaving animal *Eur. J. Neurosci.* **31** 2279–91
- [10] Zorzos A N, Boyden E S and Fonstad C G 2010 Multiwaveguide implantable probe for light delivery to sets of distributed brain targets *Opt. Lett.* **35** 4133–5
- [11] Maesoon I, Il-Joo C, Fan W, Wise K D and Euisik Y 2011 Neural probes integrated with optical mixer/splitter waveguides and multiple stimulation sites *IEEE 24th Int. Conf. on Micro Electro Mechanical Systems (MEMS) (Cancun)* pp 1051–4
- [12] Gradinaru V, Thompson K R, Zhang F, Mogri M, Kay K, Schneider M B and Deisseroth K 2007 Targeting and readout strategies for fast optical neural control *in vitro* and *in vivo* *J. Neurosci.* **27** 14231–8
- [13] Diester I, Kaufman M T, Mogri M, Pashaie R, Goo W, Yizhar O, Ramakrishnan C, Deisseroth K and Shenoy K V 2011 An optogenetic toolbox designed for primates *Nat. Neurosci.* **14** 387–97
- [14] Han X, Qian X, Bernstein J G, Zhou H-h, Franzesi G T, Stern P, Bronson R T, Graybiel A M, Desimone R and Boyden E S 2009 Millisecond-timescale optical control of neural dynamics in the nonhuman primate brain *Neuron* **62** 191–8
- [15] Gradinaru V, Mogri M, Thompson K R, Henderson J M and Deisseroth K 2009 Optical deconstruction of Parkinsonian neural circuitry *Science* **324** 354–9
- [16] Aravanis A M et al 2007 An optical neural interface: *in vivo* control of rodent motor cortex with integrated fiberoptic and optogenetic technology *J. Neural Eng.* **4** S143
- [17] Crone N E, Miglioretti D L, Gordon B and Lesser R P 1998 Functional mapping of human sensorimotor cortex with

- electrocorticographic spectral analysis: II. Event-related synchronization in the gamma band *Brain* **121** 2301–15
- [18] Schwartz A B 2004 Cortical neural prosthetics *Annu. Rev. Neurosci.* **27** 487–507
- [19] Logothetis N K, Pauls J, Augath M, Trinath T and Oeltermann A 2001 Neurophysiological investigation of the basis of the fMRI signal *Nature* **412** 150–7
- [20] Zhang J et al 2009 Integrated device for optical stimulation and spatiotemporal electrical recording of neural activity in light-sensitized brain tissue *J. Neural Eng.* **6** 055007
- [21] Rousche P and Normann R 1992 A method for pneumatically inserting an array of penetrating electrodes into cortical tissue *Ann. Biomed. Eng.* **20** 413–22
- [22] Wiebe S P and Stäubli U V 1999 Dynamic filtering of recognition memory codes in the hippocampus *J. Neurosci.* **19** 10562–74
- [23] Henyey L G and Greenstein J L 1941 Diffuse radiation in the galaxy *Astrophys. J.* **93** 70–83
- [24] Yaroslavsky A N et al 2002 Optical properties of selected native and coagulated human brain tissues *in vitro* in the visible and near infrared spectral range *Phys. Med. Biol.* **47** 2059
- [25] Wang L and Wu H-i 2007 *Biomedical Optics: Principles and Imaging* (New York: Wiley)
- [26] Zhang F, Gradinaru V, Adamantidis A R, Durand R, Airan R D, de Lecea L and Deisseroth K 2010 Optogenetic interrogation of neural circuits: technology for probing mammalian brain structures *Nat. Protoc.* **5** 439–56
- [27] Kravitz A V, Freeze B S, Parker P R L, Kay K, Thwin M T, Deisseroth K and Kreitzer A C 2010 Regulation of Parkinsonian motor behaviours by optogenetic control of basal ganglia circuitry *Nature* **466** 622–6
- [28] Cardin J A, Carlen M, Meletis K, Knoblich U, Zhang F, Deisseroth K, Tsai L-H and Moore C I 2010 Targeted optogenetic stimulation and recording of neurons *in vivo* using cell-type-specific expression of Channelrhodopsin-2 *Nat. Protoc.* **5** 247–54
- [29] Jimbo Y, Tateno T and Robinson H P C 1999 Simultaneous induction of pathway-specific potentiation and depression in networks of cortical neurons *Biophys. J.* **76** 670–8
- [30] Olsson R H III, Buhl D L, Sirota A M, Buzsaki G and Wise K D 2005 Band-tunable and multiplexed integrated circuits for simultaneous recording and stimulation with microelectrode arrays *IEEE Trans. Biomed. Eng.* **52** 1303–11
- [31] Dickey A S, Suminski A, Amit Y and Hatsopoulos N G 2009 Single-unit stability using chronically implanted multielectrode arrays *J. Neurophysiol.* **102** 1331–9
- [32] Mitzdorf U 1985 Current source-density method and application in cat cerebral cortex: investigation of evoked potentials and EEG phenomena *Physiol. Rev.* **65** 37–100
- [33] Serruya M D, Hatsopoulos N G, Paninski L, Fellows M R and Donoghue J P 2002 Brain-machine interface: instant neural control of a movement signal *Nature* **416** 141–2
- [34] Serruya M and Donoghue J 2003 Design principles of a neuromotor prosthetic device *Neuroprosthetics - Theory and Practice* vol 2, ed K W Horch and G S Dhillon (Singapore: World Scientific) pp 1158–96
- [35] Truccolo W, Donoghue J A, Hochberg L R, Eskandar E N, Madsen J R, Anderson W S, Brown E N, Halgren E and Cash S S 2011 Single-neuron dynamics in human focal epilepsy *Nat. Neurosci.* **14** 635–41